Suppression of bimolecular recombination by UV-sensitive electron transport layers in organic solar cells

Doo-Hyun Ko,[1] John R. Tumbleston,[2] Myoung-Ryul Ok,[3] Honggu Chun,[1] Rene Lopez,[2] and Edward Samulski[1,a)]

[1]*Department of Chemistry, University of North Carolina at Chapel Hill, Caudill and Kenan Laboratories, CB 3290, Chapel Hill, North Carolina 27599-3290, USA*

[2]*Department of Physics and Astronomy, University of North Carolina at Chapel Hill, Phillips Hall, CB 3255, Chapel Hill, North Carolina 27599-3255, USA*

[3]*Curriculum in Applied Sciences and Engineering, University of North Carolina at Chapel Hill, Caudill and Kenan Laboratories, CB 3290, Chapel Hill, North Carolina 27599-3290, USA*

(Received 3 June 2010; accepted 25 July 2010; published online 18 October 2010)

Incorporating UV-sensitive electron transport layers (ETLs) into organic bulk heterojunction (BHJ) photovoltaic devices dramatically impacts short-circuit current (J_{sc}) and fill factor characteristics. Resistivity changes induced by UV illumination in the ETL of inverted BHJ devices suppress bimolecular recombination producing up to a two orders of magnitude change in J_{sc}. Electro-optical modeling and light intensity experiments effectively demonstrate that bimolecular recombination, in the form of diode current losses, controls the extracted photocurrent and is directly dependent on the ETL resistivity. © *2010 American Institute of Physics*. [doi:10.1063/1.3488609]

I. INTRODUCTION

A quickly evolving approach to enhancing the efficiency of bulk heterojunction (BHJ) organic solar cells involves the insertion of additional layers between the photoactive layer and the electrodes that enhance electrical or optical characteristics.[1–7] In particular, improving the absorption of light in the photoactive layer by inserting an optical spacer layer into the device architecture enables a straightforward gain in short-circuit current (J_{sc}). This phenomenon has been demonstrated experimentally[2,5] and addressed theoretically[6,8] using a well-understood optical model. On the other hand, insertion of additional layers for electrical enhancement often modifies J_{sc}, the fill factor (FF), and the open-circuit voltage (V_{oc}),[3–5,9–13] making it difficult to decouple the fundamental physical processes involved. Even in cases where V_{oc} remains constant and the extra layer only improves J_{sc} and/or FF,[2,14–18] the relationship between the electrical properties of the additional and photoactive layer remains unclear. Herein, we demonstrate that tuning the electrical properties of an electron transport layer (ETL) adjacent to the photoactive blend determines the values of J_{sc} and FF.

In metal-insulator-metal architectures of BHJ solar cells without additional layers, performance characteristics have been directly linked to microscopic device physics that controls the photogenerated current ($J_{photo}=J_{light}-J_{dark}$). These include the two fundamental electric field-dependent loss processes that can inhibit J_{sc} and FF, namely, exciton dissociation at the donor/acceptor interface and bimolecular recombination of charge carriers.[19–21] These processes have been elucidated to identify limitations of polymer/fullerene systems like poly(3-hexylthiophene) (P3HT):phenyl-C61-butyric acid methyl ester (PCBM),[22,23] but have not been analyzed in complex cell architectures with additional non-photoactive layers. On the other hand, macroscopic parameters of the traditional photovoltaic circuit model such as the device serial resistance (R_{series}) can also dramatically alter J_{sc} and FF (Ref. 24) where the additional layers may result in unwanted parasitic losses. In order to maximize the performance of organic photovoltaics, it is essential to understand the effects of these extra layers both in terms of the microscopic processes that affect the photocurrent and in the context of the macroscopic equivalent circuit interpretation. A comprehensive understanding is prerequisite for judiciously selecting cell architectures from this fast-growing approach to solar cell fabrication.

In this paper we explore inverted organic photovoltaic (iOPV) (Ref. 25) solar cells with P3HT:PCBM as the photoactive layer. The ETL such as TiO_x,[14–16,26,27] TiO_2,[12,28,29] ZnO,[17,30,31] and Cs_2CO_3 (Ref. 11) for iOPV are necessary to operate the device by matching energy levels with the photoactive layer. In particular, the UV sensitivity of TiO_x has been studied and is known to affect iOPV device performance.[16,26] However, the relationship between the electrical properties of the ETL and the photoactive layer in the device is still elusive. We incorporate TiO_x as an ETL in an iOPV in order to exploit the temporal evolution of cell properties due to UV exposure. Our observations enable us to systematically track the variation in electrical properties associated with the ETL and the photoactive layer. We observe that after UV exposure, J_{sc} improves by two orders of magnitude while FF increases by a factor of three under solar simulated light. UV exposure does not alter the device optical performance, V_{oc}, or the P3HT:PCBM electrical properties. Hence, both the micro- and macroscopic electrical mechanisms that affect J_{sc} and FF upon insertion of an additional layer can be probed. Through the use of device modeling and light intensity experiments, we show that an in-

a)Electronic mail: et@unc.edu.

crease in the resistivity of the ETL effectively turns on bimolecular recombination that is dominated by losses related to the diode current in P3HT:PCBM.

II. EXPERIMENTAL

Indium tin oxide (ITO)-coated glass was cleaned with acetone, isopropyl alcohol and distilled water for 10 min each and then dried overnight in an oven (150 °C). The cleaned substrate was treated with UV ozone for 20 min (UVO Cleaner 42, Jelight Co. Inc.). TiO_2 sol-gel was prepared by a previously reported method[5] and spincasted on the ITO substrate and annealed at 150 °C for 1 hr in air to form an amorphous TiO_x film. For TiO_2 ETL, the spincasted film was annealed at 450 °C for 30 min in air. The sample was then moved to an inert gas (purified nitrogen) glove box where a solution of P3HT (15 mg ml^{-1}) and PCBM (12 mg ml^{-1}) in chlorobenzene was spincoated on the TiO_x or TiO_2 layer and annealed at 150 °C for 30 min. Finally the device was transferred to a vacuum chamber (2×10^{-6} torr) and 8 nm WO_3/90 nm Ag was sequentially deposited on defined cell areas (12 mm^2).

Solar cells with two different thicknesses of the TiO_x ETL (50 and 25 nm) along with devices fabricated with a TiO_2 ETL (25 nm—annealed at 450 °C for 30 min) were studied using various UV exposure times ($\lambda=365$ nm). After each UV illumination period, the device performance was measured under 85 mW/cm^2 solar simulated light using a 400 nm UV cut-off filter which was sufficient to block UV light from the solar simulator and restrict performance changes over the time of the measurement (see Ref. 32, Fig. S1 for measurement details).

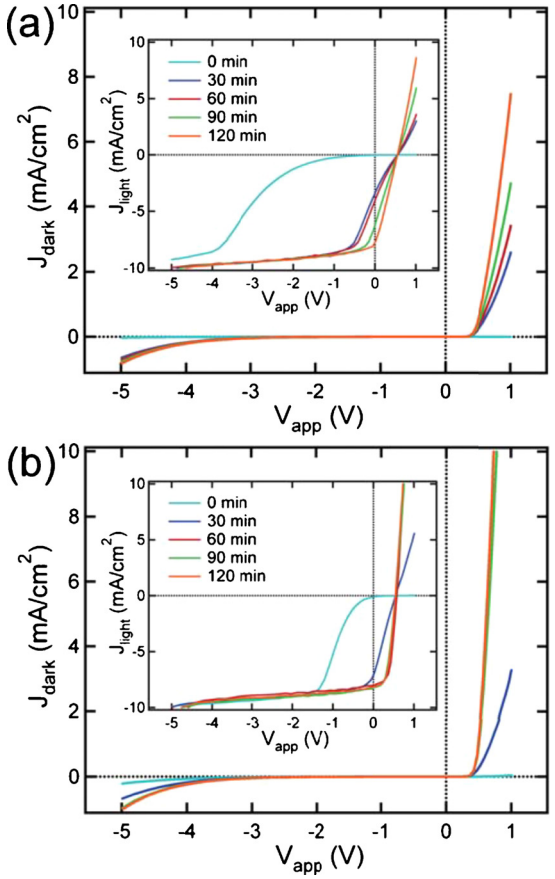

FIG. 1. (Color online) Dark current and light current (inset) densities for iOPV devices with (a) 50 nm and (b) 25 nm TiO_x ETLs under solar simulated light (with a UV cut-off filter) after successive 30 min UV ($\lambda=365$ nm) exposure times.

III. RESULTS AND DISCUSSION

Figure 1 shows that the dark (J_{dark}) and light (J_{light}) current densities in TiO_x devices undergo considerable changes after 30 min time intervals of UV illumination.[16,26] Clearly, the dark rectification, J_{sc}, and the FF are extremely poor prior to UV exposure leading to efficiencies well below 0.01%. Following consecutive UV illumination periods, performance steadily increases by more than two orders of magnitude and approaches saturation values. The UV response is somewhat sensitive to the TiO_x thickness as shown in Fig. 2 where J_{sc}, V_{oc}, FF, and R_{series} are shown after each successive 30 min exposure to UV light. Longer exposure periods are needed to achieve saturation for thicker ETLs: J_{sc} is saturated after 60 min and 120 min for devices with 25 nm and 50 nm of TiO_x, respectively. The change is most dramatic in J_{sc}, which increases from 0.07 to 8.3 mA/cm^2 after a 120 min UV exposure (25 nm TiO_x device). The FF also improves from 15% to 51% yielding an efficiency of 2.8%. However, devices with TiO_2 as the ETL are relatively insensitive to even prolonged UV illumination where the efficiency is near its saturation value prior to UV exposure (see Ref. 32, Fig. S2).

In spite of the dramatic changes observed in J_{sc} and FF, Fig. 2 also indicates that V_{oc} remains constant after each cycle of UV illumination. Furthermore, R_{series} (defined as the inverse slope of the current-voltage curves at V_{oc}) undergoes a dramatic reduction in three orders of magnitude for devices with TiO_x as the ETL. Commonly, a modification in R_{series} with constant V_{oc} is given as the primary reason for altered performance characteristics caused by the insertion of additional nonphotoactive layers.[3,4,10] However, this view does not specify the origin of the performance change. Below we provide an in-depth explanation based on fundamental optical and electrical processes associated with the iOPV device.

First, we turn our attention to photon absorption. Improvements in J_{sc} are frequently a result of increased light absorption due to a more favorable optical interference profile in the photoactive layer.[15,17] As shown in Fig. 1, at high reverse bias where electric field-dependent losses are minimized, J_{light} is constant for all devices and is consequently controlled by light absorption.[33,34] As shown in Fig. 1, the experimental photocurrent density at high reverse bias ($J_{exp.\ photo}=J_{light}-J_{dark}$) approaches a saturation value [$J_{sat}\sim9.8$ mA/cm^2; inset of Fig. 3(a)]; J_{sat} is constant for each device type and for all UV exposure times.

From these values, the generation rate of bound electron/hole pairs, G, is determined via $J_{sat}=qGL$, where q is the elementary charge and L is the active layer thickness.[33,34] An average value of $G=6.75\times10^{27}$ m^{-3} s^{-1} is obtained for all devices [Fig. 3(a)] consistent with previously reported values for P3HT:PCBM.[35] This result was checked by measuring the spectral reflection for each device and fitting it to an

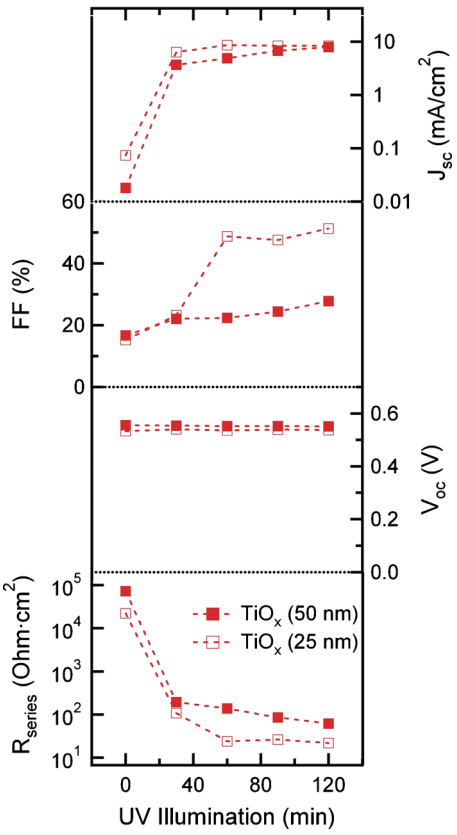

FIG. 2. (Color online) Short-circuit current (J_{sc}), FF, open-circuit voltage (V_{oc}), and series resistance (R_{series}) of devices with TiO_x as the ETL after successive 30 min intervals of UV exposure.

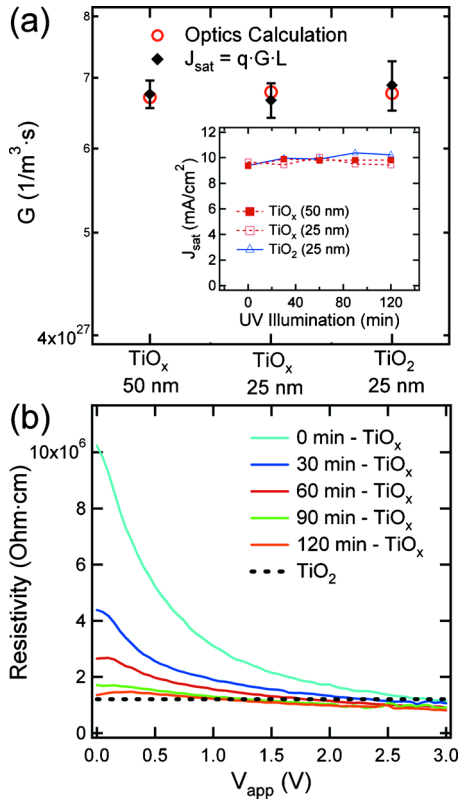

FIG. 3. (Color online) (a) Exciton generation rate, G, determined from both the saturated photocurrent J_{sat} (inset) and a separate optical reflection measurement/calculation. (b) Dark resistivity of TiO_x vs UV illumination. The resistivity of TiO_2 changes insignificantly relative to TiO_x.

optical model (see Ref. 32, Fig. S3).[36] A calculation of G values follows directly,[37] and the agreement between the two ways of determining G is shown in Fig. 3(a). This result supports the perspective that both the ETL material choice and the period of UV exposure have a negligible effect on photon absorption in the photoactive layer.[15,38] The possibility of interface effects between P3HT:PCBM and TiO_x was investigated by modifying the TiO_x interface. The interface was modified with *p*-amino benzoic acids and *p*-nitro benzoic acid, which have opposite electrostatic dipole moment orientations that can reduce recombination of carriers at the interface.[29,39,40] However, performance of the modified devices showed similar trends as the unmodified devices after cycles of UV illumination (see Ref. 32, Fig. S4). Furthermore, measurements of standard devices [Al/P3HT:PCBM/poly(3,4-ethylenedioxythiophene):poly(styrenesulfonate) (PEDOT:PSS)/ITO] and hole-only P3HT:PCBM devices (Pd/P3HT:PCBM/PEDOT:PSS/ITO) (Ref. 22) under UV illumination (see Ref. 32, Fig. S5) confirm that UV light at these levels does not significantly alter the electrical properties of P3HT:PCBM. These observations imply that UV illumination only directly influences the bulk electrical properties of the titanium oxide ETL.

The electrical properties of the ETL are characterized by measuring the dark resistivity after varying the UV illumination time for isolated layers in sandwich devices of ITO/TiO_x or TiO_2/Al with the same dimensions as the iOPV devices. As shown in Fig. 3(b), TiO_x resistivity decreases by an order of magnitude (from 1.0×10^7 to 1.2×10^6 Ω cm) for $V_{app}=0$ V, and approaches the resistivity of TiO_2 (which is almost unaffected by UV illumination). For simple metal-oxide diodes, changes in resistivity under both UV illumination and positive bias application have been attributed to an electrochemical mechanism[26,41,42] that involves the filling of negatively charged oxygen traps in the metal-oxide. The injection of free electrons and holes under forward bias and the creation of electron/hole pairs during UV illumination separately result in a free electron left behind in the conduction band of the ETL causing an increase in the conductivity. Indeed, we observed that holding the device under positive bias for specified time intervals in the dark has the same effect on device performance as UV illumination (see Ref. 32, Fig. S6).

In order to understand how a resistivity change confined to the ETL influences the physical processes in the photoactive layer, we first consider a model for standard organic BHJ solar cells that includes drift and diffusion of photogenerated carriers under the influence of bimolecular recombination that undergo a field-dependent dissociation at the donor/acceptor interface.[43] The measured changes in an isolated TiO_x or TiO_2 layer's resistivity [sandwich devices of ITO/TiO_x or TiO_2/Al; see Fig. 3(b)], in conjunction with the photoactive material's UV-independence, imply that UV exposure only affects the electrical transport properties of the ETL. Furthermore, the device V_{oc} remains constant under UV illumination indicating that the ETL energy levels are unaffected.[38] Thus, the UV effect is modeled as a change in the effective potential difference across the photoactive layer

leading to a weakening of the internal electric field. The potential boundary conditions are modified to include an ohmic voltage drop that is the product of the extracted current and a resistor. In this way, a UV-dependent serial resistance is incorporated into the model and used as a fitting parameter to approximate the current-voltage data in the first and forth quadrants. Series resistance values fall within 20% of the measured values in Fig. 2. Other model parameters describing P3HT:PCBM are taken as constant including the exciton generation rate [Fig. 3(a)], carrier mobilities, dielectric constant, and built-in voltage.[35] The model simulations are shown in Fig. 4(a) where the trends of Fig. 2 for V_{oc}, J_{sc}, and FF are reproduced. The model is then used to calculate the spatially averaged percentage of photogenerated free carriers that undergo bimolecular recombination ($\langle BR_{photo} \rangle$) for each UV illumination time. These results are shown in Fig. 4(b) where it is observed that longer UV exposure times leads to an increased internal electric field and reduced bimolecular recombination.

At first glance it appears that recombination of photogenerated carriers is the primary cause of the reduced current output. However, its relative importance may be probed by setting $\langle BR_{photo} \rangle = 0$ for all applied voltages. Interestingly, this recombination pathway has little effect on the extracted current as shown in Fig. 4(a) for 30 min UV exposures. The current at short-circuit is modified by less than 8%. This result is primarily due to the fact that recombined carriers first form a bound electron-hole pair before decaying to the ground state, which has some probability of dissociation back into free charges.[34] The probability of exciton dissociation is near 90% at short-circuit for standard P3HT:PCBM devices meaning that most of the free carriers that recombine will again dissociate back to free carriers making this a minimal loss process.[22] Furthermore, we do not attribute UV-dependent current losses to exciton dissociation due to its weak dependence on the internal electric field[22] and demonstrated negligible loss for P3HT:PCBM solar cells near open-circuit conditions.[44]

The relative unimportance of these loss mechanisms on the photocurrent indicates that J_{photo} may be approximated as constant for all applied voltages. A simple replacement circuit model may then be used as is frequently done with BHJ devices, especially P3HT:PCBM:[24,45,46]

$$J = J_o\left[\exp\left(\frac{e(V_{app} - JR_{series})}{nk_BT}\right) - 1\right] + \frac{(V_{app} - JR_{series})}{R_{shunt}} - J_{photo}, \quad (1)$$

where J_0 is the reverse saturation current, e is the elementary charge, n is the diode ideality factor, k_B is Boltzmann's constant, T is the temperature, V_{app} is the applied voltage, R_{shunt} is the shunt resistance, R_{series} is the series resistance, J is the current density, and J_{photo} is the photogenerated current that is constant with applied voltage. The first term on the right-hand side constitutes J_{diode}.

As with the drift-diffusion model, fits to the experimental current-voltage curves in the 1st and 4th quadrants are obtained by varying R_{series}. These curves show negligible deviations from the drift-diffusion model of Fig. 4(a) and are

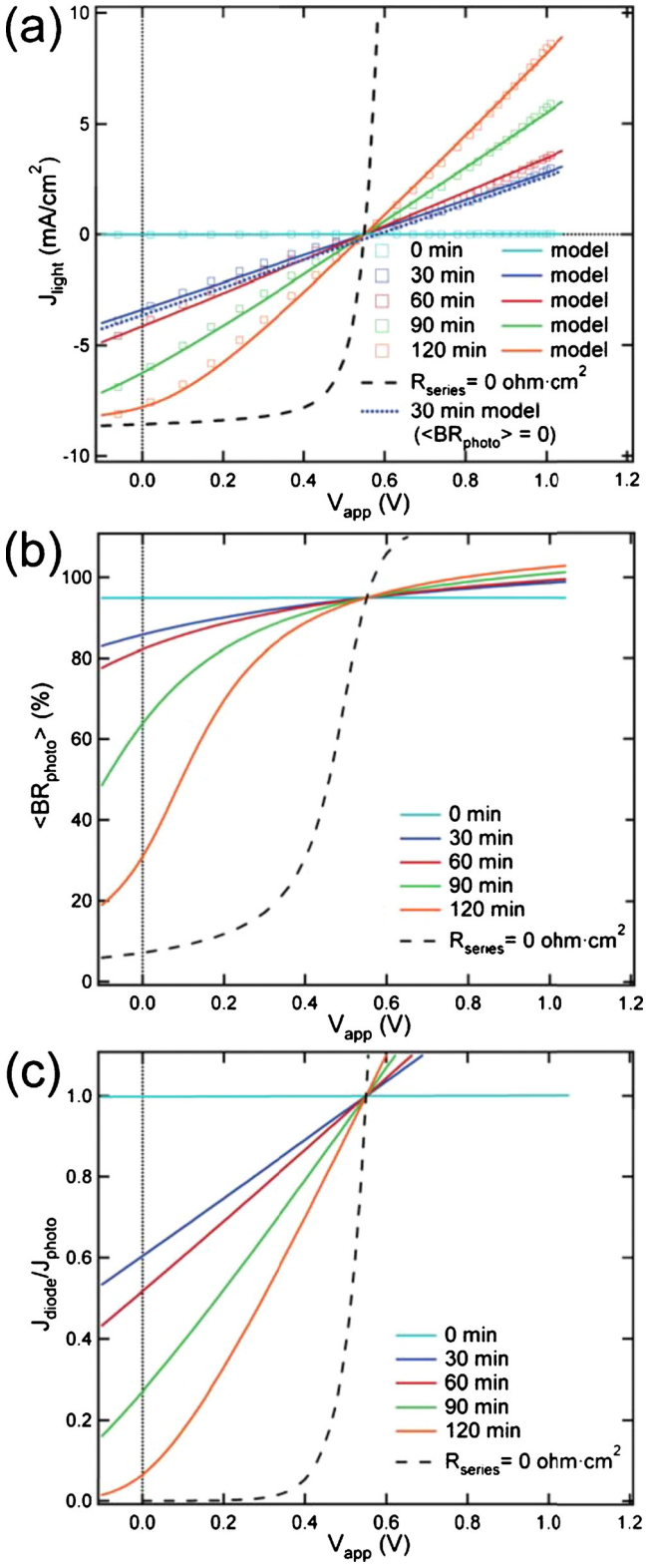

FIG. 4. (Color online) (a) Experimental and simulated light current density (J_{light}) for each cycle of UV illumination. The importance of bimolecular recombination in the photocurrent is shown by setting $\langle BR_{photo} \rangle = 0$ for 30 min UV illumination. (b) Calculated spatial average of BR_{photo} as a function of V_{app} for each UV illumination cycle, which gives the fraction of free carriers that recombine via this loss process. (c) The ratio of J_{diode} to J_{photo} given by the equivalent circuit model. All panels show the results for an ideal P3HT:PCBM device where $R_{series} = 0\ \Omega\ cm^2$.

not shown. Other model parameters including the reverse saturation current ($J_o = 2.0 \times 10^{-4}$ mA/cm^2) and diode ideality factor (n=2.0) (Ref. 47) that describe the diode current (J_{diode}), shunt resistance ($R_{shunt} = 5.0 \times 10^5$ Ω cm^2), and photogenerated current ($J_{photo} = 8.5$ mA/cm^2) remain unchanged in each simulation. The case where $R_{series} = 0$ Ω cm^2 is also displayed showing that further reduction would primarily result in a higher FF. The primary utility of this model is the calculation of J_{diode}, so that a comparison can be made with J_{photo}. In the power generating regime of the current-voltage curve (i.e., fourth quadrant), high levels of J_{diode} will cause a reduction in current in the external circuit. For example, the ratio J_{diode}/J_{photo} is unity at V_{oc}. Recently, J_{diode} has been microscopically understood to be a bimolecular recombination process that resembles BR_{photo} described above for the drift-diffusion model, but is related to the inherent diode function instead of the photogenerated current.[44,47] Therefore, we interpret J_{diode} as a bimolecular recombination process (BR_{diode}) that is separate from BR_{photo}. The ratio J_{diode}/J_{photo} is given in Fig. 4(c) where the effect of high values for R_{series} can be quickly understood. For each UV exposure time, this ratio is unity at V_{oc} where all J_{photo} "flows" through the diode and recombines. Likewise, for no (0 min) UV illumination where $R_{series} \geqslant 0$, the ratio is close to unity over the entire forward bias range. As the device is illuminated with UV light, the series resistance decreases along with the ratio J_{diode}/J_{photo}. Ultimately this causes a reduction in BR_{diode}.

The significance of BR_{photo} in limiting J_{photo} can be probed by measuring J_{sc} over a range of light intensities where a nonlinear dependence signals the prevalence of this process.[22,48,49] When measuring a device with high serial resistance, this tendency is also expected from the circuit model. Due to the UV-controlled series resistance observed here, the relationship between J_{sc} and light intensity should become increasingly linear for prolonged UV illumination. This prediction is observed as shown in Fig. 5(a) where J_{sc} is given as a function of light intensity under λ=532 nm laser illumination. The data are fit to the circuit model by varying only R_{series} using the same diode and shunt parameters as in Fig. 4. Sublinear behavior is observed beginning below 1 mW/cm^2 for the 30 min UV illuminated device, and at higher intensity (above 1 mW/cm^2) for the device where the performance becomes UV saturated (~120 min). By assuming $J_{sc} \propto I^{\alpha}$ where I is the light intensity, we find by fitting the power law between 10 and 100 mW/cm^2, that α takes respective values of 0.38 and 0.73 for 30 and 120 min of UV illumination. As with the current-voltage data, the ratio J_{diode}/J_{photo} [Fig. 5(b)] demonstrates the relative impact of BR_{diode} for each UV illumination time. Regardless of UV exposure, J_{sc} is increasingly affected by diode losses under higher light intensity. Furthermore, exposure to UV effectively determines the intensity where losses in the diode become significant. It follows that these are nearly the same light intensities where nonlinearity in the extracted current begins.

Light intensity measurements prior to UV illumination are not shown due to the high measurement variability from extremely low currents. Therefore, the incident photon to current conversion efficiency (IPCE) measured with a lock-in amplifier is shown in Fig. 5(c). The IPCE involves intensities near 0.05 mW/cm^2 where the effect of the diode current will be weak relative to higher light intensities. Integration of IPCE to calculate J_{sc} (Refs. 2 and 50) gives values of 3.5 mA/cm^2 and 7.6 mA/cm^2 for the device prior to UV illumination and after 120 min UV exposure, respectively. By contrast, $J_{sc} < 0.1$ mA/cm^2 prior to UV illumination as

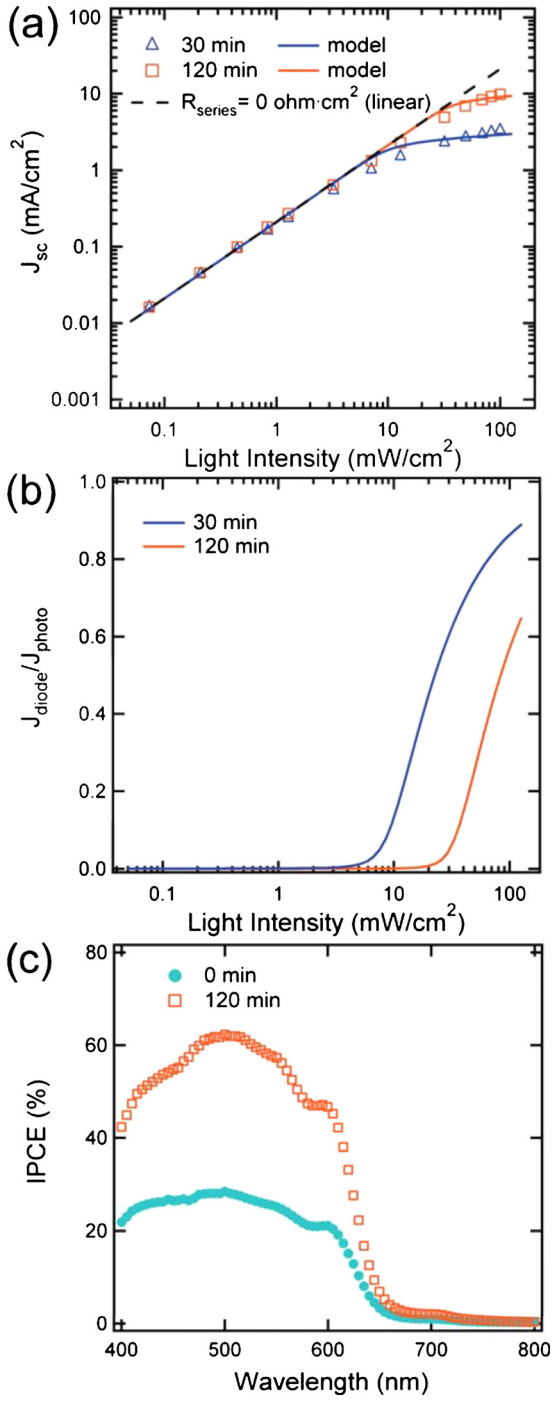

FIG. 5. (Color online) (a) J_{sc} as a function of λ=532 nm laser light intensity for a device with TiO_x as the ETL after 30 min and 120 min UV exposure. The prediction from the circuit model is also given for each UV illumination time along with the linear dependence for $R_{series} = 0$ Ω cm^2. (b) Model calculation of the ratio J_{diode}/J_{photo} for each illumination time. (c) IPCE prior to UV illumination and after UV saturation where the incident light intensity is ~0.05 mW/cm^2.

measured under solar simulated light (Fig. 2). The gross overestimation of the predicted J_{sc} from the IPCE measurement results from the dominance of BR_{diode} near 1 sun conditions where the current does not scale linearly with light intensity. We can now conclude that the electrical properties of the TiO_x ETL effectively determines bimolecular recombination as quantified by diode losses in P3HT:PCBM. Prior to UV illumination, the high layer resistivity drives more photogenerated current through the diode, which in turn, leads to extremely high levels of recombination mimicking device operation at open-circuit. Prolonged UV exposure reduces the ETL resistivity, which lowers the serial resistance resulting in reduced recombination losses.

IV. CONCLUSION

In this work, we have shown that the electrical properties of nonphotoactive layers significantly affect physical processes in the BHJ material. Improvements in J_{sc} that span two orders of magnitude originate from a resistivity drop in the ETL induced by UV illumination. The resistivity has a profound effect on serial resistance, which effectively controls bimolecular recombination attributed to the diode current.

ACKNOWLEDGMENTS

Support for this work is from NSF (Solar: Grant No. DMR-0934433) and from UNC-Chapel Hill Institute for the Environment Carolina Energy Fellow. Acknowledgment is made to the donors of The American Chemical Society Petroleum Research Fund (PRF) (Grant No. 49187-DNI10) for partial support of this research. We thank Professor Frank Tsui, Will Rice, Matt Wolboldt, Dr. Matthew K. Brennaman, Ralph L. House, Dr. Kwan Skinner, and Dr. Ethan Klem for stimulating conversations.

[1] J. Y. Kim, K. Lee, N. E. Coates, D. Moses, T.-Q. Nguyen, M. Dante, and A. J. Heeger, Science **317**, 222 (2007).
[2] S. H. Park, A. Roy, S. Beaupre, S. Cho, N. Coates, J. S. Moon, D. Moses, M. Leclerc, K. Lee, and A. J. Heeger, Nat. Photonics **3**, 297 (2009).
[3] S. Chaudhary, H. Lu, A. M. Muller, C. J. Bardeen, and M. Ozkan, Nano Lett. **7**, 1973 (2007).
[4] M. D. Irwin, D. B. Buchholz, A. W. Hains, R. P. H. Chang, and T. J. Marks, Proc. Natl. Acad. Sci. U.S.A. **105**, 2783 (2008).
[5] J. Y. Kim, S. H. Kim, H. H. Lee, K. Lee, W. Ma, X. Gong, and A. J. Heeger, Adv. Mater. **18**, 572 (2006).
[6] J. Gilot, I. Barbu, M. M. Wienk, and R. A. J. Janssen, Appl. Phys. Lett. **91**, 113520 (2007).
[7] H.-L. Yip, S. K. Hau, N. S. Baek, H. Ma, and A. K. Y. Jen, Adv. Mater. **20**, 2376 (2008).
[8] B. V. Andersson, D. M. Huang, A. J. Moule, and O. Inganas, Appl. Phys. Lett. **94**, 043302 (2009).
[9] M.-H. Park, J.-H. Li, A. Kumar, G. Li, and Y. Yang, Adv. Funct. Mater. **19**, 1241 (2009).
[10] C. Tao, S. Ruan, X. Zhang, G. Xie, L. Shen, X. Kong, W. Dong, C. Liu, and W. Chen, Appl. Phys. Lett. **93**, 193307 (2008).
[11] G. Li, C. W. Chu, V. Shrotriya, J. Huang, and Y. Yang, Appl. Phys. Lett. **88**, 253503 (2006).
[12] C. Tao, S. Ruan, G. Xie, X. Kong, L. Shen, F. Meng, C. Liu, X. Zhang, W. Dong, and W. Chen, Appl. Phys. Lett. **94**, 043311 (2009).
[13] V. Shrotriya, G. Li, Y. Yao, C.-W. Chu, and Y. Yang, Appl. Phys. Lett. **88**, 073508 (2006).
[14] C. Waldauf, M. Morana, P. Denk, P. Schilinsky, K. Coakley, S. A. Choulis, and C. J. Brabec, Appl. Phys. Lett. **89**, 233517 (2006).
[15] T. Ameri, G. Dennler, C. Waldauf, P. Denk, K. Forberich, M. C. Scharber, C. J. Brabec, and K. Hingerl, J. Appl. Phys. **103**, 084506 (2008).
[16] R. Steim, S. A. Choulis, P. Schilinsky, and C. J. Brabec, Appl. Phys. Lett. **92**, 093303 (2008).
[17] A. K. K. Kyaw, X. W. Sun, C. Y. Jiang, G. Q. Lo, D. W. Zhao, and D. L. Kwong, Appl. Phys. Lett. **93**, 221107 (2008).
[18] H.-W. Tsai, Z. Pei, and Y.-J. Chan, Appl. Phys. Lett. **93**, 073310 (2008).
[19] P. W. M. Blom, V. D. Mihailetchi, L. J. A. Koster, and D. E. Markov, Adv. Mater. **19**, 1551 (2007).
[20] R. A. Marsh, C. R. McNeill, A. Abrusci, A. R. Campbell, and R. H. Friend, Nano Lett. **8**, 1393 (2008).
[21] A. Gonzalez-Rabade, A. C. Morteani, and R. H. Friend, Adv. Mater. **21**, 3924 (2009).
[22] V. D. Mihailetchi, H. X. Xie, B. de Boer, L. J. A. Koster, and P. W. M. Blom, Adv. Funct. Mater. **16**, 699 (2006).
[23] R. Häusermann, E. Knapp, M. Moos, N. A. Reinke, T. Flatz, and B. Ruhstaller, J. Appl. Phys. **106**, 104507 (2009).
[24] J. D. Servaites, S. Yeganeh, T. J. Marks, and M. A. Ratner, Adv. Funct. Mater. **20**, 97 (2010).
[25] L.-M. Chen, Z. Hong, G. Li, and Y. Yang, Adv. Mater. **21**, 1434 (2009).
[26] T. Kuwabara, T. Nakayama, K. Uozumi, T. Yamaguchi, and K. Takahashi, Sol. Energy Mater. Sol. Cells **92**, 1476 (2008).
[27] C. S. Kim, S. S. Lee, E. D. Gomez, J. B. Kim, and Y.-L. Loo, Appl. Phys. Lett. **94**, 113302 (2009).
[28] C.-Y. Li, T.-C. Wen, T.-H. Lee, T.-F. Guo, J.-C.-A. Huang, Y.-C. Lin, and Y.-J. Hsu, J. Mater. Chem. **19**, 1643 (2009).
[29] S. K. Hau, H.-L. Yip, O. Acton, N. S. Baek, H. Ma, and A. K. Y. Jen, J. Mater. Chem. **18**, 5113 (2008).
[30] S. K. Hau, H.-L. Yip, N. S. Baek, J. Zou, K. O'Malley, and A. K. Y. Jen, Appl. Phys. Lett. **92**, 253301 (2008).
[31] M. S. White, D. C. Olson, S. E. Shaheen, N. Kopidakis, and D. S. Ginley, Appl. Phys. Lett. **89**, 143517 (2006).
[32] See supplementary material at http://dx.doi.org/10.1063/1.3488609 for description of device fabrication and measurement, performance of device with TiO_2 as the ETL, optical simulations, measurement of standard P3HT:PCBM and hole-only devices, the electrochemical mechanism of UV illumination, and electrical simulations.
[33] A. M. Goodman and A. Rose, J. Appl. Phys. **42**, 2823 (1971).
[34] V. D. Mihailetchi, L. J. A. Koster, J. C. Hummelen, and P. W. M. Blom, Phys. Rev. Lett. **93**, 216601 (2004).
[35] L. J. A. Koster, V. D. Mihailetchi, and P. W. M. Blom, Appl. Phys. Lett. **88**, 093511 (2006).
[36] G. Dennler, K. Forberich, M. C. Scharber, C. J. Brabec, I. Tomis, K. Hingerl, and T. Fromherz, J. Appl. Phys. **102**, 054516 (2007).
[37] J. D. Kotlarski, P. W. M. Blom, L. J. A. Koster, M. Lenes, and L. H. Slooff, J. Appl. Phys. **103**, 084502 (2008).
[38] C. Uhrich, D. Wynands, S. Olthof, M. K. Riede, K. Leo, S. Sonntag, B. Maennig, and M. Pfeiffer, J. Appl. Phys. **104**, 043107 (2008).
[39] C. Goh, S. R. Scully, and M. D. McGehee, J. Appl. Phys. **101**, 114503 (2007).
[40] H. Haick, M. Ambrico, T. Ligonzo, and D. Cahen, Adv. Mater. **16**, 2145 (2004).
[41] M. Takahashi, K. Tsukigi, T. Uchino, and T. Yoko, Thin Solid Films **388**, 231 (2001).
[42] F. Verbakel, S. C. J. Meskers, and R. A. J. Janssen, J. Appl. Phys. **102**, 083701 (2007).
[43] L. J. A. Koster, E. C. P. Smits, V. D. Mihailetchi, and P. W. M. Blom, Phys. Rev. B **72**, 085205 (2005).
[44] C. G. Shuttle, B. O'Regan, A. M. Ballantyne, J. Nelson, D. D. C. Bradley, and J. R. Durrant, Phys. Rev. B **78**, 113201 (2008).
[45] P. Schilinsky, C. Waldauf, J. Hauch, and C. J. Brabec, J. Appl. Phys. **95**, 2816 (2004).
[46] C. Waldauf, P. Schilinsky, J. Hauch, and C. J. Brabec, Thin Solid Films **451–452**, 503 (2004).
[47] C. G. Shuttle, A. Maurano, R. Hamilton, B. O'Regan, J. C. de Mello, and J. R. Durrant, Appl. Phys. Lett. **93**, 183501 (2008).
[48] W. U. Huynh, J. J. Dittmer, N. Teclemariam, D. J. Milliron, A. P. Alivisatos, and K. W. J. Barnham, Phys. Rev. B **67**, 115326 (2003).
[49] L. J. A. Koster, V. D. Mihailetchi, H. Xie, and P. W. M. Blom, Appl. Phys. Lett. **87**, 203502 (2005).
[50] J. Nelson, *The Physics of Solar Cells* (Imperial College Press, London, 2003).